Chemistry and Physics of Lipids 160 (2009) 85–97

Contents lists available at ScienceDirect

Chemistry and Physics of Lipids

journal homepage: www.elsevier.com/locate/chemphyslip

The solid–liquid phase diagrams of binary mixtures of consecutive, even saturated fatty acids

Mariana C. Costa[a,b], Mariana Sardo[b], Marlus P. Rolemberg[c], João A.P. Coutinho[b], Antonio J.A. Meirelles[d], Paulo Ribeiro-Claro[b], M.A. Krähenbühl[a,*]

[a] LPT, Department of Chemical Process, School of Chemical Engineering, University of Campinas, UNICAMP, P.O. Box 6066, 13083-970 Campinas, SP, Brazil
[b] CICECO, Departamento de Química da Universidade de Aveiro, 3810-193 Aveiro, Portugal
[c] DETQI, Department of Chemical Technology, Universidade Federal do Maranhão (UFMA), São Luís, Maranhão, Brazil
[d] EXTRAE, Department of Food Engineering, School of Food Engineering, University of Campinas, UNICAMP, P.O. Box 6121, 13083-862 Campinas, SP, Brazil

ARTICLE INFO

Article history:
Received 18 January 2008
Received in revised form 19 February 2009
Accepted 19 May 2009
Available online 9 June 2009

Keywords:
Solid–liquid equilibrium
Saturated fatty acids
Phase diagram
DSC
XRD
FT–Raman

ABSTRACT

For the first time, the solid–liquid phase diagrams of five binary mixtures of saturated fatty acids are here presented. These mixtures are formed of caprylic acid ($C_{8:0}$) + capric acid ($C_{10:0}$), capric acid ($C_{10:0}$) + lauric acid ($C_{12:0}$), lauric acid ($C_{12:0}$) + myristic acid ($C_{14:0}$), myristic acid ($C_{14:0}$) + palmitic acid ($C_{16:0}$) and palmitic acid ($C_{16:0}$) + stearic acid ($C_{18:0}$). The information used in these phase diagrams was obtained by differential scanning calorimetry (DSC), X-ray diffraction (XRD), FT–Raman spectrometry and polarized light microscopy, aiming at a complete understanding of the phase diagrams of the fatty acid mixtures. All of the phase diagrams reported here presented the same global behavior and it was shown that this was far more complex than previously imagined. They presented not only peritectic and eutectic reactions, but also metatectic reactions, due to solid–solid phase transitions common in fatty acids and regions of solid solution not previously reported. This work contributes to the elucidation of the phase behavior of these important biochemical molecules, with implications in various industrial applications.

1. Introduction

Fatty acids have aroused the interest of researchers since the early 1900s because they are the major components of oils and fats (Karleskind, 1996). Lately, an accrued interest in these compounds has resulted from their application in the production of coatings, plastics, cleaning products (Johnson and Fritz, 1989), phase change materials for energy storage (Zhang et al., 2001; Shilei et al., 2006) and biodiesel (Falk and Meyer-Pittroff, 2004; Meher et al., 2006).

Due to the applications of fatty acids in the chemical, food and pharmaceutical industries (Carvalho et al., 2006; Kogan and Garti, 2006), knowledge about their properties and phase behavior could induce innovations in many branches of these industries, especially in the food industry, due to the influence of the phase behavior and crystalline habit of the fatty acid mixtures on the characteristics of consumer products, such as confectionary fats.

The polymorphism of triglycerides and fatty acids has been known for a long time, but the study of the crystal forms of pure fatty acids only began around 1950 and to this day is still a challenging task (Vand et al., 1951; Holland and Nielsen, 1963; Lomer, 1963; Goto and Asada, 1978a,b; Kaneko et al., 1990; Moreno et al., 2007). Researchers have been concerned about both the study of the properties and the behavior of fats and glycerides in the solid phase (Chapman, 1962; Timms, 1984; Garti and Sato, 1989; Sato et al., 1999; Sato, 2001), and the phase diagrams of fats (Bailey, 1950; Timms, 1984; Small, 1986; Sato et al., 1999; Sato, 2001) and fatty acids (Inoue et al., 2004a; Inoue et al., 2004b; Inoue et al., 2004c; Costa et al., 2007b).

The existence of invariant points, such as eutectic and peritectic points, in mixtures of saturated fatty acids has already been reported (Bailey, 1950; Small, 1986), but in recent works by the present authors (Costa et al., 2007a,b), the presence of these invariant points was also observed in mixtures for which the difference in carbon atom number between the chains was inferior to 6. The phase diagrams of binary mixtures of fatty acids were believed to be simply eutectic for systems with chain length differences equal or larger to 6 carbon atoms, whilst for the others the presence of an intermediate compound, unstable at the melting point, originated a peritectic point (Small, 1986; Iwahashi et al., 2005). Recent results concerning the phase diagrams of binary systems of dicarboxylic acids have shown the complexity of these systems below the *liquidus* line (Ventola et al., 2006; Ventola et al., 2008). The phase diagrams reported the presence of eutec-

* Corresponding author. Tel.: +55 19 3521 3964; fax: +55 19 3521 3965.
E-mail addresses: mccosta@feq.unicamp.br (M.C. Costa), msardo@ua.pt (M. Sardo), marlus@ufma.br (M.P. Rolemberg), jcoutinho@ua.pt (J.A.P. Coutinho), tomze@fea.unicamp.br (A.J.A. Meirelles), prc@ua.pt (P. Ribeiro-Claro), mak@feq.unicamp.br (M.A. Krähenbühl).

0009-3084/$ – see front matter © 2009 Elsevier Ireland Ltd. All rights reserved.
doi:10.1016/j.chemphyslip.2009.05.004

tic, peritectic and metatectic and several monophasic regions, and biphasic solid–solid and solid–liquid domains. The complexity of the phase diagrams of dicarboxylic acids suggested that the phase diagrams of fatty acids should also be very complex. As a consequence the phase diagrams of the binary mixtures of the fatty acids determined using the DSC technique, were reviewed, and a number of indications that they were far more complex than previously admitted were found. To confirm these indications other techniques were used to elucidate the complete phase diagrams of the binary mixtures of fatty acids, below the saturation line.

This is part of a series of studies concerning the solid–liquid equilibrium (SLE) of fatty acid binary mixtures. In the present study the phase diagrams of binary mixtures of saturated fatty acids with a difference of two carbon atoms between the chains, were established using DSC measurements complemented by FT–Raman spectroscopy, X-ray diffraction studies and polarized light microscopy. It will be shown that, as expected from what had been observed with similar systems (Ventola et al., 2006, 2008; Moreno et al., 2007), the phase diagram of these mixtures was far more complex than previously admitted.

2. Experimental

2.1. Materials

The standards used to calibrate the DSC were indium (99.99%) certified by TA instruments (United States); cyclohexane (min 99.9%) and naphthalene (min 99%), both from Merck (Germany). The fatty acids used to prepare the samples were of high purity and were obtained from the following suppliers with no further purification: caprylic acid (min 99%), capric acid (min 99%), lauric acid (99–100%), myristic acid (99–100%) and palmitic acid (min 99%) – Sigma–Aldrich (United States); stearic acid (min 97%) – Merck (Germany) was used in the DSC analysis and stearic acid (min 99%) – Sigma–Aldrich (United States) was used in the other analyses. Commercial nitrogen (99.99%, used for preparing the binary samples) and high purity nitrogen (99.9999%, used in the calorimeter) were supplied by Air Liquide (Brazil).

2.2. Methods

2.2.1. Preparation of the fatty acid binary mixtures

Samples of 1 g of the fatty acid mixtures were prepared for the compositions only studied by DSC. For the compositions studied by multiple techniques, 3–5 g samples were prepared according to the following methodology: an amount of each fatty acid was weighed on an analytical balance (Adam AAA/L) with ±0.2 mg accuracy, to obtain a desired molar fraction, generally an interval of 0.1 molar fraction, with an uncertainty of ±0.0002. The compounds weighed were placed in vials and heated to 10 K above the highest melting point of the components. While heating, the samples were mixed using a magnetic stirrer in an atmosphere of nitrogen. The temperature limit and the nitrogen atmosphere were adopted to avoid oxidation of the fatty acids. The mixtures were then allowed to cool, naturally, to room temperature (298.15 K) and kept in a freezer at 273 K until further analysis.

For the FT–Raman spectra recorded before melting (BM) the samples were just weighed and mixed in the solid state by crushing the crystals in a mortar. The melting of these samples was carried out in the spectrophotometer inside the capillary tube used for the analysis after recording the BM spectra, at a temperature circa to 10 K above the melting point of the heaviest compound. The samples were then cooled inside the spectrophotometer, naturally, to the temperature required to acquire the spectra after mixing the compounds in the liquid phase and allowing for the formation of new mixed crystals.

2.2.2. Differential scanning calorimetry (DSC)

The solid–liquid equilibrium of the pure fatty acids and their mixtures were characterized by DSC using a MDSC 2920 TA Instruments calorimeter, equipped with a refrigerated cooling system which, in this study, operated between 258 K and 423 K. Samples (2–5 mg) of each mixture were weighed in a microanalytical balance (PerkinElmer AD6) with an accuracy of $\pm 0.2 \times 10^{-5}$ mg, and put in sealed aluminum pans. In order to erase previous thermal histories, each sample was submitted to an initial heating run at 5.0 K min^{-1}, initiated at ambient temperature (298.15 K) and continuing until a temperature 15 K above the highest melting point of the components was reached. After 20 min at this temperature, the samples were cooled to 25 K below the lowest melting point of the components, at a cooling rate of 1.0 K min^{-1}, and allowed to stay at this temperature for 30 min. After this pre-treatment each sample was analyzed in a heating run at a heating rate of 1.0 K min^{-1}. Peak top temperatures were measured for pure fatty acids and for the fatty acid mixtures using a universal analysis program of TA instruments. Peak top temperatures were also considered to determine the temperature of phase transitions associated with overlapped peaks.

Eq. (1) was used to calculate the average of absolute deviations (AAD) between the measurements. The AAD were estimated to be inferior to 0.2 K (Costa et al., 2007b).

$$\mathrm{AAD} = \frac{1}{n}\sum_{i=1}^{n} |T_{i,\mathrm{lit}} - T_{i,\mathrm{exp}}| \quad (1)$$

Through the phase diagram constructed by DSC was possible to make a choice of compositions and temperatures, bellow the liquidus line, that would be investigate by other techniques. So, the *desired temperature* mentioned in the following sections is the temperature selected through the phase diagram, generally between two transitions detected by DSC.

2.2.3. Polarized light microscopy

A Leica (DM LM) light microscope was used to acquire the images. The images at ambient temperature were obtained using a polarized lens and transmitted light. The samples were prepared by melting the sample between two coverslips.

The images at controlled temperatures were obtained by putting the sample on a coverslip on a hot FP82H stage connected to the central processor unit of the Mettler Toledo FP 90 DSC. The central processor unit was programmed to heat the sample at a heating rate of 0.1 K min^{-1}, initiating at the ambient temperature, 298.15 K, until the melting of the sample was reached. Images were acquired with a magnification of 50 times at each 0.5 K, or when the sample presented modifications.

2.2.4. X-ray diffraction

The fatty acid diffractograms were obtained using a Philips X'Pert equipment operating in the reflection mode with Cu Kα (λ = 1.5406 Å). The cool chamber was an Anton Paar TTK450, the temperature controller a TCU100 and the chamber was cooled using liquid nitrogen. Diffraction data were collected in the 2θ range from 4° to 50° in steps of 0.02 and a time per step of 2 s, with incident and diffracted beams with anti-scatter slits of 1°, receiving slit of 0.1 mm and a curved graphite diffracted beam monochromator. The diffractograms acquired for these mixtures did not have sufficient resolution to allow for the crystal structures to be derived from them. They were only used to identify differences between the solid regions.

The sample were heating or cooling until the desired temperature at which the diffraction data were collected between 273.15 K and 340 K with no thermal treatment. The heating or cooling process of the sample was conduct by the temperature controller with no programmed temperature.

2.2.5. FT–Raman spectroscopy

The spectra were recorded using a RFS-100 Bruker FT-Spectrometer equipped with a Nd:YAG laser with an excitation wavelength of 1064 nm and the laser power set to 400 mW. Each spectrum corresponded to the measurement of 400 scans and 2 cm^{-1} resolution.

In some experiments, it has been reported that the sample temperature can increase significantly due to laser exposure (Marigheto et al., 1996; Johansson et al., 2002), which may subsequently lead to polymorphic transformations. Aiming to evaluate the effect of sample heating during the measurements, a sample of each fatty acid was exposed continuously to 400 mW of laser power for 4 h, during which several 5 min records were collected at room temperature (295.15 K). A comparison of the spectra showed that no change due to laser irradiation occurred in this time interval. Using 400 mW laser power, all the FT–Raman spectra were collected in 45 min or less.

The samples were sealed in Kimax glass capillary tubes (0.8 mm i.d.) and the temperature variation studies were carried out in the 273–353 K range with a commercial Harney–Miller-type assembly, the temperature being monitored by the resistivity of a calibrated thermocouple. Under these circumstances, the error in temperature was estimated to be less than 0.5 K, with fluctuations during each recording below 1 K.

2.2.5.1. Ab initio calculations. *Ab initio* calculations are a trustworthy method used to perform and confirm the assignment of the bands observed experimentally. The vibrational frequencies and intensities of the lauric, myristic, and stearic acids were obtained from *ab initio* calculations for both the monomer and dimer forms according to the PiMM methodology (Nolasco et al., 2006). The calculations were performed using the G03W program package (Frisch et al., 2003) run on a personal computer. The fully optimized geometry, harmonic vibrational wavenumbers and infrared and Raman intensities were obtained at the B3LYP level (Lee et al., 1988; Becke, 1993), using the standard 6-31G* basis set (Harihara and Pople, 1973). This approach was proven to provide a good quality/computational cost ratio (Vaz and Ribeiro-Claro, 2005a,b; Nolasco et al., 2006). The harmonic vibrational wavenumbers were scaled by a factor of 0.9614 (Scott and Radom, 1996) for comparison with the experimental values, and the calculated harmonic wavenumbers were scaled by a factor of 0.9614 (Scott and Radom, 1996) to account for anharmonicity and electron correlation effects. Vibrational assignments were based on the atomic displacements and calculated intensities.

The phase transitions were established from the DSC thermograms and the visual observation using the microscopy. The diffractograms acquired for these mixtures did not have sufficient resolution to allow for the crystal structures to be derived from them. The spectroscopic techniques were only used to identify and confirm differences between the solid phases in the multiple regions identified on the phase diagrams.

3. Results

Although the results presented below are mostly related to the lauric acid + myristic acid system, studies were also carried out for the other binaries to confirm these results, but will not be reported here to avoid overloading the report.

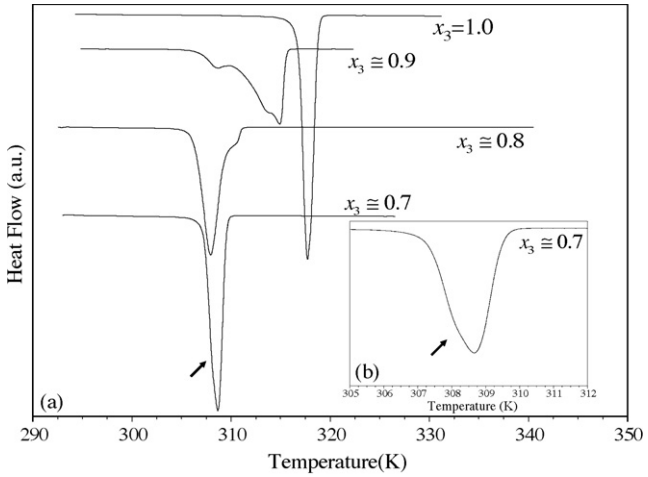

Fig. 1. (a) Differential thermal curves for the system lauric acid (3) + myristic acid (4); (b) inset of the differential thermal curve for $x_3 \cong 0.70$.

3.1. Thermal analysis

All the thermograms from previously published data (Francis et al., 1937; Grondal and Rogers, 1944; Bailey, 1950; Müller and Stage, 1961; Costa et al., 2007a,b) along with new data not previously published for systems that differ by two carbon atoms in their chain length, were reinterpreted. Figs. 1 and 2 present the thermograms of the system lauric acid (3) + myristic acid (4) and caprylic acid (1) + capric acid (2) respectively, and are examples of the complexity of the phase diagram of the fatty acid systems, due the existence of several overlapping peaks.

Tables 1–5 show the temperatures of phase transition and melting of the systems studied here along with the enthalpies associated with the major phase transitions that were possible to individualize.

3.2. FT–Raman spectroscopy

The FT–Raman spectra show different vibration modes for the different crystal forms of the fatty acids and their melting (Brown et al., 1987; Garti and Sato, 1989; Tandon et al., 2000). Although the changes in composition and temperature of the samples could be observed in the whole spectrum, the present study was focused on the three main spectral regions: 100–300 cm^{-1},

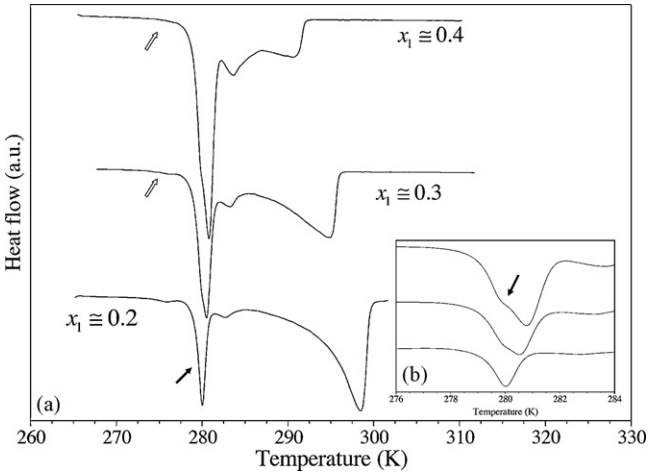

Fig. 2. (a) Differential thermal curves of the system caprylic acid (1) + capric acid (2); (b) inset of the differential thermal curve around the eutectic composition.

Table 1
Solid–liquid equilibrium data for caprylic acid (1) + capric acid (2) system.

x_1 (molar fraction)	$T_{melting}$ (K)	ΔH_{sample} (kJ mol mix^{-1})	$T_{peritectic}$ (K)	$\Delta H_{peritectic}$ (kJ mol mix^{-1})	$T_{metatectic}$ (K)	$T_{eutectic}$ (K)	$\Delta H_{eutectic}$ (kJ mol mix^{-1})	T_{trans1} (K)	T_{trans2} (K)	T_{trans3} (K)	$T_{trans.pure}$ (K)
0.0000	304.42	28.20									
0.1000	301.89	25.49	279.36	1.71	281.81						
0.1999	298.54	17.05	280.02	3.81	282.80			275.75			
0.3000	294.98	12.10	280.53	7.55	283.29			276.04	279.98		
0.4001	291.21	4.35	280.86	11.99	283.64				279.79	289.40	
0.5000	286.84	0.40	281.28	14.60	283.30	276.73	2.85				
0.5994	280.63	11.89				277.41	8.88				
0.6997	278.36	8.92				277.13	10.49				
0.7998	281.91	1.70				276.88	17.74			278.79	
0.8998	285.96	11.02				277.73	4.21			281.25	
1.0000	289.63	22.34									287.72

Table 2
Solid–liquid equilibrium data for capric acid (2) + lauric acid (3) system.

x_2 (molar fraction)	$T_{melting}$ (K)	ΔH_{sample} (kJ mol mix^{-1})	$T_{peritectic}$ (K)	$\Delta H_{peritectic}$ (kJ mol mix^{-1})	$T_{metatectic}$ (K)	$T_{eutectic}$ (K)	$\Delta H_{eutectic}$ (kJ mol mix^{-1})	T_{trans1} (K)	T_{trans2} (K)	T_{trans3} (K)	$T_{trans.pure}$ (K)
0.0000	318.07	38.70									317.56
0.1010	314.86	32.11	296.30	1.22	299.52						
0.1993	311.94	24.85	296.95	5.59	299.45						
0.2999	309.12	15.86	297.29	11.10	299.54			295.56		306.37	
0.4001	304.82	3.96	296.95	17.24	299.52			296.05		303.05	
0.4457	302.8	0.88	297.16	10.13	299.38	292.76	0.16				
0.5002	299.06	2.23				293.36	2.86				
0.5530	296.77	9.16				293.02	4.53				
0.5989	296.31	5.20				293.55	8.16				
0.6529	295.33	3.64				293.95	9.73				
0.7001	294.75	9.08				293.27	17.01				
0.7516	294.35					293.37	12.65				
0.7998	298.15	3.66				293.07	7.36		294.49		
0.9000	301.94	19.64							294.53	300.23	
1.0000	304.42	28.20									

1350–1550 cm^{-1} and 2800–3050 cm^{-1}, as shown in Fig. 3 for the lauric acid (3) + myristic acid (4) system.

To evaluate if the solid phase region of the phase diagrams was composed of the pure fatty acids plus an intermediate compound, as suggested by some authors (Bailey, 1950; Small, 1986), physical mixtures of the pure compounds were prepared and their Raman spectra collected before melting the sample, and compared with the spectra collected after melting and recrystallization of the sample. Fig. 4 shows the Raman spectra for the lauric acid (3) + myristic acid (4) system at 305 K before (physical mixture, dashed line) and after (solid line) sample melting, in the three spectral regions mentioned above.

3.3. X-ray diffraction

Fig. 5 shows the diffraction patterns at 298.15 K for different compositions of the lauric acid (3) + myristic acid (4) system in the ranges of $7.5^\circ \leq 2\theta \geq 10^\circ$ and $18^\circ \leq 2\theta \geq 26^\circ$. The first important observation was the similarities between the diffraction patterns of the pure fatty acids and those of the mixtures $x_3 \cong 0.95$ and $x_3 \cong 0.05$. Both mixtures presented almost the same diffraction pattern, except for the disappearance of some very small peaks present in the pure fatty acid in which the mixture was richer.

Also, in Fig. 5, for $x_3 \cong 0.15$, it was possible to observe the appearance of new peaks at $2\theta \cong 9^\circ$ and $2\theta \cong 23^\circ$. These peaks could be attributed to a new phase that, with the increase in concentration of the lauric acid, coexisted with other phases due to the coexistence of these new peaks with the previously referred to myristic phase, and after reaching a certain value for the lauric acid concentration, the new peaks coexisted with the peaks related to the lauric acid phase.

The effect of temperature on the diffractograms was evaluated for the same compositions mentioned above. Unfortunately most solid phases present very similar powder diffractograms, mak-

Table 3
Solid–liquid equilibrium data for lauric acid (3) + myristic acid (4) system.

x_3 (molar fraction)	$T_{melting}$ (K)	ΔH_{sample} (kJ mol mix^{-1})	$T_{peritectic}$ (K)	$\Delta H_{peritectic}$ (kJ mol mix^{-1})	$T_{metatectic}$ (K)	$T_{eutectic}$ (K)	$\Delta H_{eutectic}$ (kJ mol mix^{-1})	T_{trans1} (K)	$T_{trans.pure}$ (K)
0.0000	328.88	48.35							328.18
0.1004	325.72	41.23	310.04	0.83	312.19				
0.1997	323.24	32.50	310.55	7.00	312.55				
0.3002	319.08	14.29	310.88	14.66	312.69			318.22	
0.4001	314.79	8.24	310.9	21.72	312.84				
0.5002	310.96	34.92				308.1	4.27		
0.6002	310.42	24.39				308.34	10.68		
0.6400	309.7	31.02				308.23	32.05		
0.7001	308.66					308.05	34.38		
0.7996	310.61					307.92	32.13		
0.8996	314.93	28.44				308.5	5.06	313.47	
1.0000	318.07	48.35							317.56

Table 4
Solid–liquid equilibrium data for myristic acid (4) + palmitic acid (5) system.

x_4 (molar fraction)	$T_{melting}$ (K)	ΔH_{sample} (kJ mol mix^{-1})	$T_{peritectic}$ (K)	$\Delta H_{peritectic}$ (kJ mol mix^{-1})	$T_{metatectic}$ (K)	$T_{eutectic}$ (K)	$\Delta H_{eutectic}$ (kJ mol mix^{-1})	T_{trans} (K)	$T_{trans.pure}$ (K)
0.0000	335.44	55.85							
0.0490	335.41	48.46							
0.1010	334.06	36.69	320.05	0.99	322.29				
0.1510	332.87	24.34	320.63	3.22	322.54				
0.2020	331.87	20.18	320.85	5.54	322.71				
0.2517	330.77	17.21	320.96	8.09	322.76			328.60	
0.3027	329.63	12.62	321.21	11.64	323.02			326.94	
0.3491	328.01	8.14	321.43	15.78	323.15			325.64	
0.4002	326.00	2.50	321.17	20.58	322.96				
0.4499	321.27	41.03				318.62	1.22		
0.5023	321.75	36.71				319.06	4.04		
0.5505	321.99	34.15				319.32	5.55		
0.6044	321.18	15.98				319.30	7.55		
0.6498	320.64	10.13				319.38	17.32		
0.6984	320.42	8.91				319.59	27.38		
0.7203						319.96	21.97		
0.8499	324.04	4.57				319.74	17.75	322.02	
0.9004	325.54	13.29				319.60	8.28	324.00	
1.0000	328.88	44.01					1.22		328.18

Table 5
Solid–liquid equilibrium data for palmitic acid (5) + stearic acid (6) system.

x_5 (molar fraction)	$T_{melting}$ (K)	ΔH_{sample} (kJ mol mix^{-1})	$T_{peritectic}$ (K)	$\Delta H_{peritectic}$ (kJ mol mix^{-1})	$T_{metatectic}$ (K)	$T_{eutectic}$ (K)	$\Delta H_{eutectic}$ (kJ mol mix^{-1})	T_{trans} (K)	$T_{trans.pue}$ (K)
0.0000	343.98	67.56							343.31
0.1004	341.61	60.64	329.77	3.55	331.55				
0.2000	339.79	47.44	330.11	13.17	331.77			338.53	
0.2999	337.49	33.07	330.31	25.27	332.00			334.83	
0.4001	333.90	6.40	330.46	49.21	332.19				
0.4997	330.76	46.79				328.47	5.77		
0.5998	330.38	40.63				328.74	14.34		
0.6996						329.06	54.27		
0.7991	329.86	18.79				328.90	33.31		
0.8815	333.64	38.39				329.01	13.40	332.12	
1.0000	335.44	55.85							

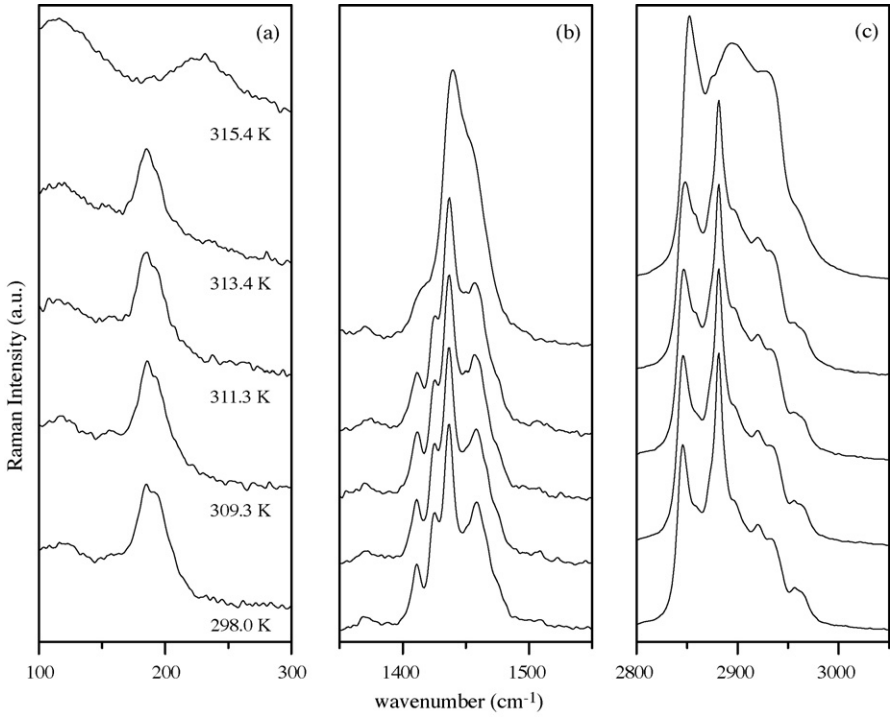

Fig. 3. Temperature dependence of the FT–Raman spectra for lauric acid (3) + myristic acid (4) system at $x_3 \cong 0.30$: (a) range 100–300 cm^{-1}; (b) range 1350–1550 cm^{-1}; (c) range 2800–3000 cm^{-1}.

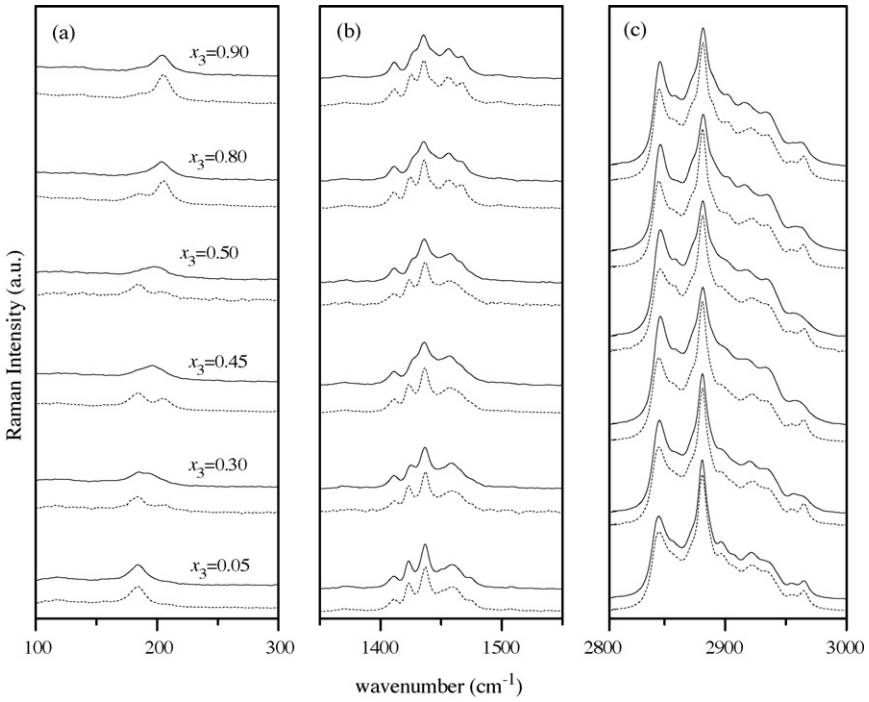

Fig. 4. FT–Raman spectra for lauric acid (3) + myristic acid (4) system at 305 K. The dashed lines represent the spectra before melting and the solid lines after melting. The compositions for figures b and c are the same presented in figure a.

ing it very hard to distinguish between them and to observe the solid–solid transitions present in the phase diagram. Fig. 6 shows an example of the similarities between different phases for $x_3 \cong 0.95$ with an increase in temperature. With this composition just a small shift of the peak at $2\theta \cong 23^\circ$ was observed. On the other hand, for $x_3 \cong 0.40$, as presented in Fig. 7, the changes in the diffraction pattern are very clear. In this case the diffraction patterns showed that with an increase in temperature from 309.15 K to 312.15 K, some peaks disappeared and the broadening of the remaining peaks and the form of the baseline denounced the presence of a liquid phase at 312.15 K.

3.4. Polarized light microscopy

Temperature scans of a number of mixtures of the samples were carried out using polarized light microscopy. Fig. 8 presents the micrographs for the system lauric acid (3) + myristic acid (4) at $x_3 \cong 0.40$, in the temperature range between 309 K and 318 K, while heating the sample at 0.1 K min^{-1}.

Fig. 8a shows the sample still in the completely solid state, where crystals in thin overlapped layers can be seen, presenting an irregular shape. With an increase in the temperature to between 312.15 K and 313.55 K (Fig. 8b–d), the objects in the image became

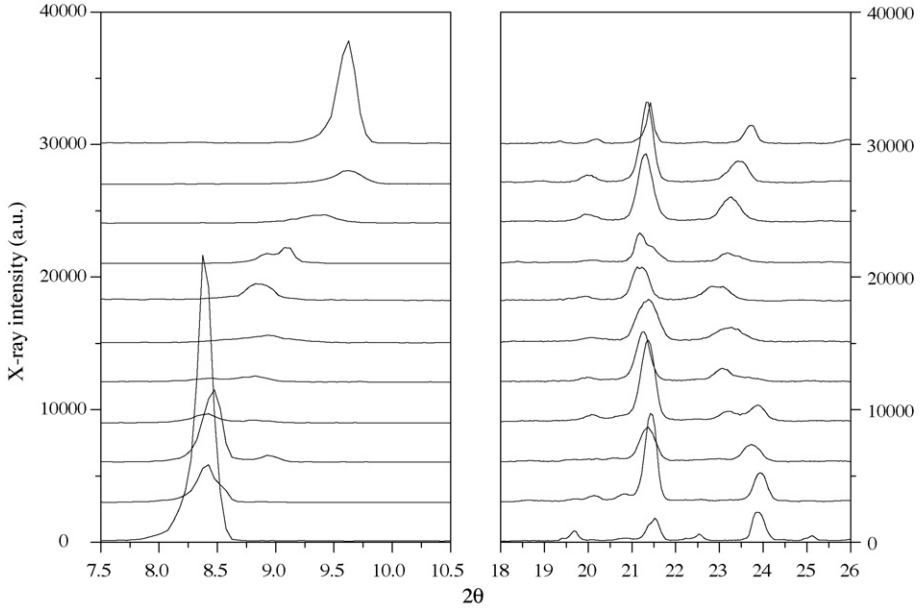

Fig. 5. X-ray powder diffraction patterns for the system lauric acid (3) + myristic acid (4) at T = 309.15 K. From top to bottom: x_3 = 1.00, $x_3 \cong 0.95$, $x_3 \cong 0.80$, $x_3 \cong 0.60$, $x_3 \cong 0.50$, $x_3 \cong 0.40$, $x_3 \cong 0.25$, $x_3 \cong 0.15$, $x_3 \cong 0.05$ and $x_3 \cong 0.00$; (a) range $7^\circ \leq 2\theta \geq 10^\circ$; (b) range $18^\circ \leq 2\theta \geq 26^\circ$.

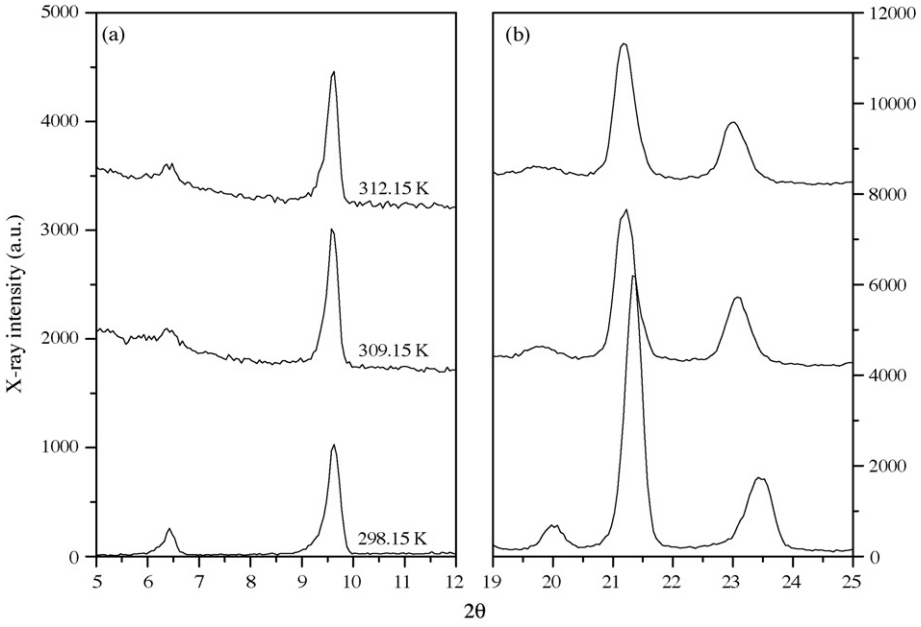

Fig. 6. X-ray powder diffraction patterns for the system lauric acid (3) + myristic acid (4) at constant composition $x_3 \cong 0.95$.

brighter and their shape became rounder, due to partial melting of the crystals. With a further increase in the temperature, the liquid formed was observed to undergo recrystallization, and in Fig. 8f, no liquid can be observed, and the small quantities of liquid previously formed are now in the solid state as shown by their irregular shape, characteristic of a solid, as indicated by the black arrow in the figure. At 316 K (Fig. 8g), the sample was partially melted, and the last image (Fig. 8h) shows a picture of the completely melted sample.

4. Discussion

The deviations between the melting temperature data obtained in this study and the data previously published were calculated using Eq. (1). The deviations were small, showing good agreement between the saturation line here reported and that measured by other authors.

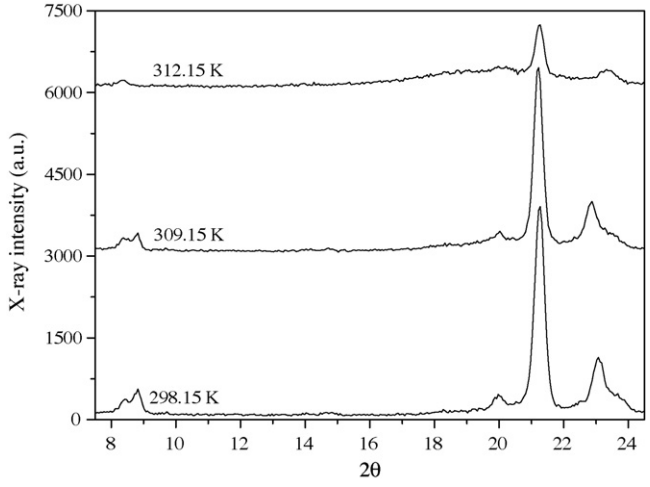

Fig. 7. X-ray powder diffraction patterns for the system lauric acid (3) + myristic acid (4) at constant composition $x_3 \cong 0.40$. From top to bottom: $T = 312.15$ K, $T = 309.15$ K and 298.15 K.

According to the classification of Nývlt (1977) the phase diagram of binary mixtures of consecutive even saturated fatty acids is similar to a type 2-Ib2 diagram, and the same interpretation was adopted previously both by us and by others (Grondal and Rogers, 1944; Bailey, 1950; Müller and Stage, 1961; Small, 1986; Costa et al., 2007b). According to this conventional interpretation, the phase diagram of the lauric acid (3) + myristic acid (4) system presents six regions, in which the pure solid myristic acid or lauric acid coexist with a liquid mixture or with the intermediate compound formed (Costa et al., 2007b), the phase diagram presenting two invariant points: a peritectic point and a eutectic point.

The thermograms of the binary systems studied immediately after mixing suggest the complexity of these phase diagrams. The thermograms presented in Figs. 1 and 2 as examples, show some subtle, not easily identifiable, transitions, making the task of interpretating and consequently originating a complex phase diagram, difficult. Fig. 1 presents the thermograms for some mixtures of the lauric acid (3) + myristic acid (4) system. In this figure three peaks for $x_3 \cong 0.90$ are clearly identifiable but for $x_3 \cong 0.70$ the existence of more than one peak is observed on the expansion of the thermogram in the inset. While the existence of more than one peak for $x_3 \cong 0.70$ only shows that the eutectic point is not exactly at this composition, the presence of three peaks for $x_3 \cong 0.90$ was not expected according to the conventional interpretation of these phase diagrams, and up to the present moment, remains unexplained.

Fig. 2 presents the thermograms for the system caprylic (1) + capric acid (2) for $x_1 \cong 0.20$, $x_1 \cong 0.30$ and $x_1 \cong 0.40$. One can observe the existence of a small peak, marked with a white arrow, in the curve for $x_1 \cong 0.20$, which decreases with increase in the caprylic acid concentration, until it disappears at $x_1 \cong 0.40$. For the same system, the expansion of the major peaks, marked with a black arrow in Fig. 2b, shows the presence of two overlapping peaks. These overlapping peaks disappear close to the peritectic point at $x_1 \cong 0.50$. These endothermic peaks observed in Figs. 1 and 2 are related to transitions in the solid phase (Ventola et al., 2006; Moreno et al., 2007). Overlapping peaks, such as those shown in Figs. 1 and 2, were found in most of the thermograms obtained in this study, throughout almost the entire concentration range, indicating that

these systems present complex phase diagrams, as observed for the dicarboxylic acids (Ventola et al., 2006, 2008) and previously suggested by Bailey (1950).

Plotting the enthalpies of the peaks associated with the eutectic and peritectic points reported in Tables 1–5, as a function of the composition of the mixture (Tamman plot), one can identify the concentration ranges of the two phase regions associated with these points (Chernik, 1995; Inoue et al., 2004a,b). Fig. 9 shows the Tamman plot for the lauric acid (3) + myristic acid (4) system, and it can be seen that none of the biphasic regions extended to the pure compounds, indicating that a region of complete mutual solubility existed at the extremes of the phase diagram.

The thermograms of the fatty acid binary systems showed: (i) the existence of complete mutual solubility at the extremes of the

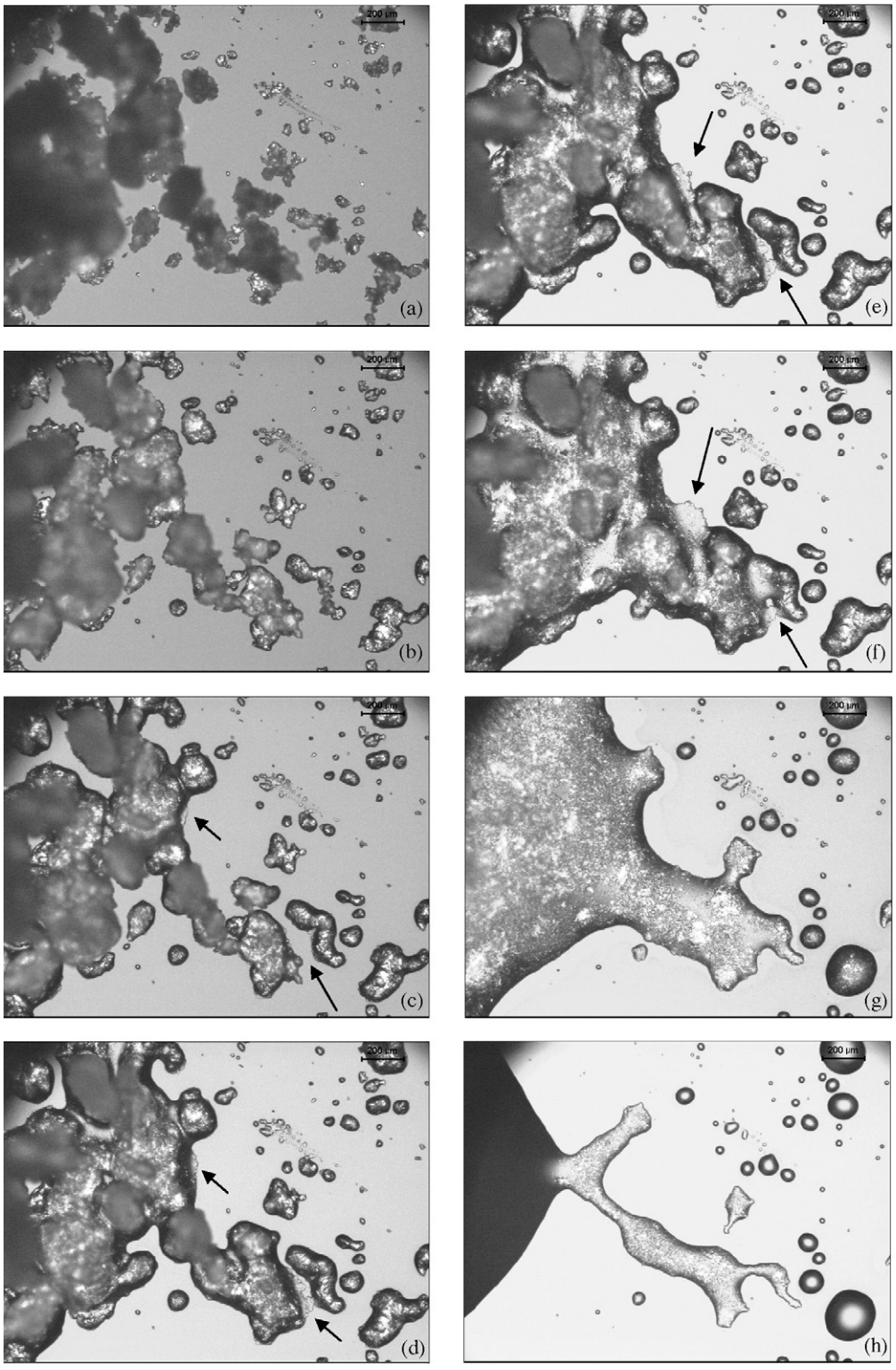

Fig. 8. Light microscopy images of the system lauric acid (3) + myristic acid (4) at $x_3 \cong 0.40$. (a) 309.15 K; (b) 312.15 K; (c) 313.15 K; (d) 313.55 K; (e) 313.75 K; (f) 314.15 K; (g) 316.15 K and (h) 318.15 K.

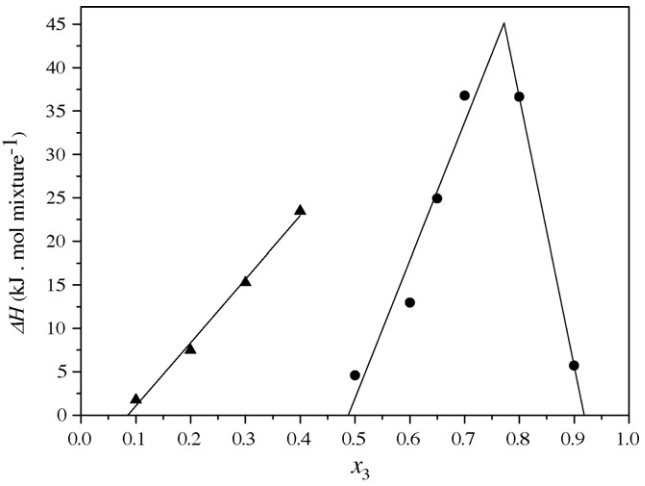

Fig. 9. Tamman plot for lauric acid (3) + myristic acid (4) system. (▲) Enthalpy of the peritectic reaction; (●) enthalpy of the eutectic reaction; (—) fitting to the experimental results obtained.

phase diagram, (ii) the presence of other solid–solid transitions beyond those related to the eutectic and peritectic reactions.

To allow for a correct interpretation of the Raman spectra, the assignment of the bands related to the pure acids was based on *ab initio* calculations for monomers and dimers, according to methodology described elsewhere (Nolasco et al., 2006). The Raman spectra of the pure acids were found to be mainly described by the spectrum calculated for the corresponding monomer. Notable exceptions were the bands related to the carboxylic group (which can be qualitatively described by the dimer spectra) and the bands arising from Fermi resonance. The final assignments given were in general agreement with previous, empirical assignments (Brown et al., 1987).

The FT–Raman spectra provide information about the conformational arrangement of the molecules in both the crystal and liquid forms, especially with respect to the spectra of the crystal forms, in which the first region, Fig. 3a, is dominated by the strong band assigned to the LAM-3 vibrational mode (longitudinal acoustic mode – CCC angle deformation). This moderately sharp band was no longer observed in the melted sample, thus providing a means to monitor the solid–liquid phase transition.

The 1350–1550 cm^{-1} region, Fig. 3b, is ascribed to CH_2 and CH_3 bending modes. It has also been found to be sensitive to temperature variations and phase transition. In particular, both the higher wavenumber component at *ca.* 1460 cm^{-1} – assigned to the CH_3 bending mode – and the low wavenumber bands at *ca.* 1410 cm^{-1} and 1425 cm^{-1} – assigned to CH_2 bending modes – lose their intensity with increases in temperature. In the spectra of the liquid phase, these bands were only observed as shoulders of the central band.

In the third region, shown in Fig. 3c, 2800–3050 cm^{-1}, only the bands ascribed to the CH stretching modes (νCH) were expected. However, these modes are severely disturbed by several Fermi resonances (Lewis and McElhaney, 2000), leading to a complex band profile. The whole profile was sensitive to both temperature variation and phase transition. The intensity ratio of the two main peaks in the crystal phase at *ca.* 2845 cm^{-1}, related to the symmetrical CH_2 stretching mode, and at *ca.* 2881 cm^{-1}, assigned to the asymmetric CH_2 stretching mode, has been used to evaluate the *trans*/*gauche* conformational ratio within the carbon chains (Lewis and McElhaney, 2000). In addition, the Fermi resonance components at higher wavenumbers are strongly intensified in the liquid phase, providing a clear distinction between the crystal phase and liquid phase band profiles.

Fig. 4 shows the Raman spectra for the lauric acid (3) + myristic acid (4) system at a temperature of 305 K, with increasing concentrations of lauric acid (3). As can be seen in Fig. 4a, the two LAM-3 bands belonging to myristic acid (≅185 cm^{-1}) and to lauric acid (≅205 cm^{-1}) can be seen in the spectra of the physical mixtures (BM) for all the compositions (due to the low concentration, only weak bands are observed for $x_3 = 0.05$ and $x_3 = 0.90$). However, after melting and recrystallization at the same temperature, only a single band with its maximum at an intermediate value between those of the pure acids, was observed, clearly indicating that, after melting, the mixture was no longer a physical mixture of two pure solids. If a pure eutectic system, as previously admitted for these systems, was observed, the two spectra should be identical. This is not the case what shows that the structure of the phase diagrams previously reported is not correct.

The same behavior was observed in the 1400–1500 cm^{-1} region (Fig. 4b). While the band at *ca.* 1410 cm^{-1} remained nearly unchanged, the band at *ca.* 1425 cm^{-1} shifted upwards and lost its intensity after sample melting and recrystallization. This effect was not clear for $x_3 \cong 0.05$, but became more evident for compositions with larger x_3. The νC–H region (Fig. 4c) provides additional information concerning the nature of the samples after melting. In comparison with the physical mixture, the spectra of the samples after melting presented a decrease in the (2881 cm^{-1})/(2845 cm^{-1}) intensity ratio and a moderate increase in intensity for the higher wavenumber side of the band profile (*ca.* 2900–2950 cm^{-1}). These effects seem to have an onset at $x_3 > 0.05$ and present a maximum at $x_3 \cong 0.45$. Both effects were associated with an increase in the conformational disorder. In particular the decrease in the (2881 cm^{-1})/(2845 cm^{-1}) intensity ratio indicated an increase in the *gauche* conformations within the carbon chain probably associated with defects at the lamellar interface of the Ci phase, as discussed by Dorset (2004). The effect was even more dramatic at higher temperatures.

The FT–Raman results observed for the various systems studied were not compatible with a simple phase diagram of the type 2-Ib2 as previously accepted, and together with the thermograms previously reported depict a more complex phase diagram.

The X-ray diffraction was another technique used to understand the phase diagram of the fatty acid systems. Although some papers about the polymorphism of pure fatty acids can be found in the

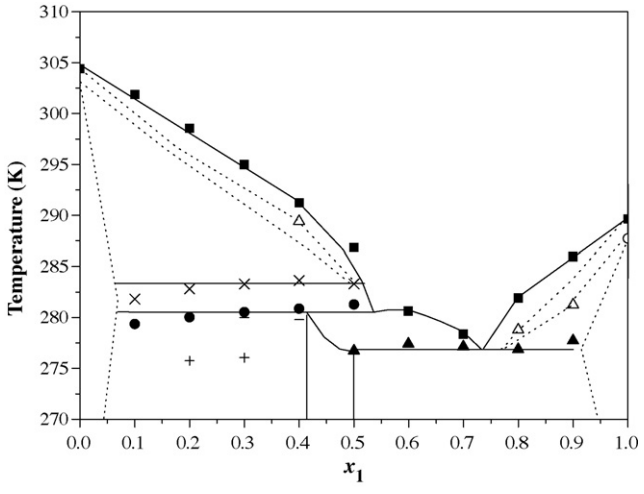

Fig. 10. Phase diagram of the system caprylic acid (1) + capric acid (2). (■) Fusion temperature; (●) peritectic temperature; (▲) eutectic temperature; (×) metatectic temperature; (+, –, △) transitions temperatures on the solid phase; (○) transition on the solid phase of the pure component.

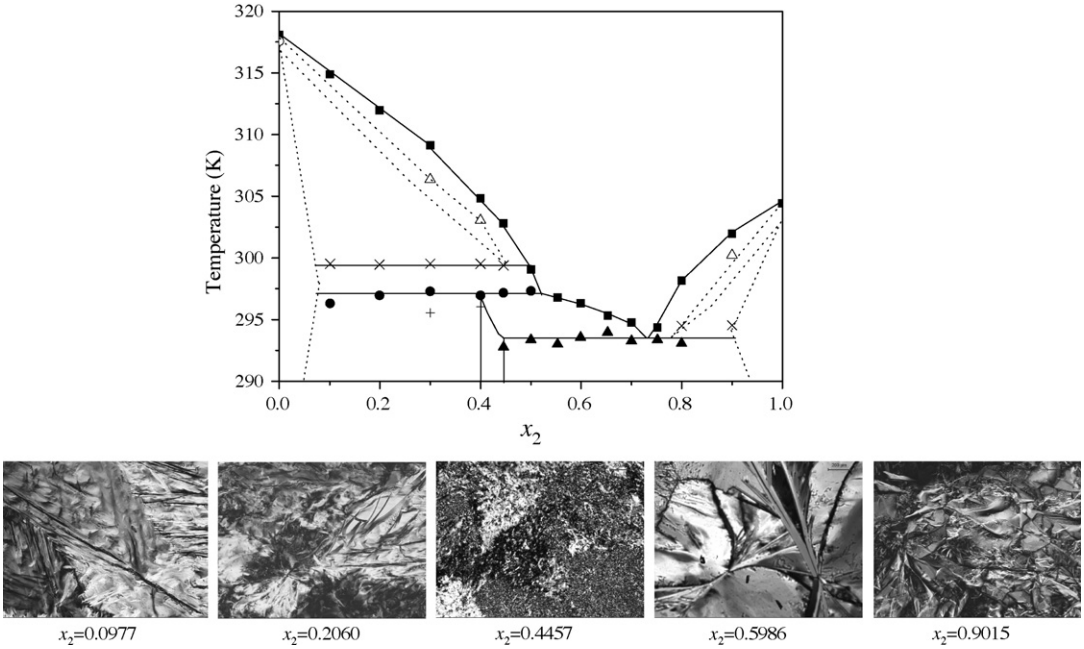

Fig. 11. Phase diagram of the system capric acid (2) + lauric acid (3) and light microscopy images of the same system at different compositions. (■) Fusion temperature; (●) peritectic temperature; (▲) eutectic temperature; (×) metatectic temperature; (+, –, △) transitions temperatures on the solid phase; (◯) transition on the solid phase of the pure component.

literature (Vand et al., 1951; Holland and Nielsen, 1963; Lomer, 1963; Goto and Asada, 1978a,b; Garti and Sato, 1989; Kaneko et al., 1990; Moreno et al., 2007), all mentioning the existence of at least three different crystal forms in pure fatty acids, the study of the solid phase of fatty acid mixtures is a difficult task because of the different polymorphs and multiple solid phases that seem to be present. The diffractograms obtained in the present study for the pure fatty acids were in good agreement with the work of Moreno et al. (2007).

The diffraction patterns obtained for the compositions of $x_3 \cong 0.05$ and $x_3 \cong 0.95$ are similar to those of the pure fatty acids, myristic acid and lauric acid respectively. Without any evidence of the presence of lauric acid in the composition of $x_3 \cong 0.05$ and without any evidence of the presence of myristic acid in $x_3 \cong 0.95$ as presented in Fig. 5, the existence of a monophasic region of solid solution, named C, at the extremes of the phase diagram is sustained, along with the Tamman plot.

The appearance of new peaks at $2\theta \cong 9^\circ$ and $2\theta \cong 23^\circ$ as observed in Fig. 5, can be related to the formation of a new phase, Ci, which coexisted with the C phase at $x_3 \cong 0.15$, and for which the peaks observed at $x_3 \cong 0.05$ were still present. With the increase in concentration of lauric acid in the mixture for $x_3 \cong 0.40$, the peaks related to the Ci phase became more intense, while those related to the C phase, $2\theta \cong 8^\circ$ and $2\theta \cong 24^\circ$, lost their intensity. In the region between $0.45 \leq x_3 \leq 0.50$ only one peak was observed at $2\theta \cong 9^\circ$ and at $2\theta \cong 23^\circ$, indicating the existence of a monophasic region, Ci, with complete miscibility of the two fatty acids. With the increase in lauric acid concentration, at $x_3 \cong 0.60$ another peak, $2\theta \cong 9.3^\circ$, corresponding to the C phase observed in the lauric acid rich region, appeared and coexisted with the Ci phase up to concentrations close to $x_3 \cong 0.95$ where, as discussed above, only a peak akin to that of the pure lauric acid, although less intense, was observed.

The shift observed in the diffraction pattern with the increase in temperature, Fig. 6, is one more indication of the existence of a region of complete miscibility at the extreme of the phase diagram at 298.15 K, and the passage to a region where two phases, C and C_h, coexist above 309.15 K. The increase in temperature caused a rearrangement of the molecules in the crystal cell, originating a new crystal form. This transition was similar to that observed by Ventolá et al. for dioic acids (Ventola et al., 2006, 2008).

The diffraction patterns presented in Fig. 7 show the presence of a liquid phase at 312.15 K, as observed by the broadening of the peaks and the form of the baseline. It can also be observed that the peaks corresponding to the Ci phase disappeared at this temperature.

The diffractograms indicated that the phase diagrams of the mixtures studied in the present work consisted of (i) two regions of complete miscibility at the extremes of the phase diagram, C; (ii) one monophasic region, Ci, at about $0.40 \leq x_a \leq 0.50$; (iii) two solid–solid regions separated by the Ci region; (iv) a solid–liquid equilibrium region, C + l, delimited by the peritectic temperature, eutectic temperature and the monophasic region.

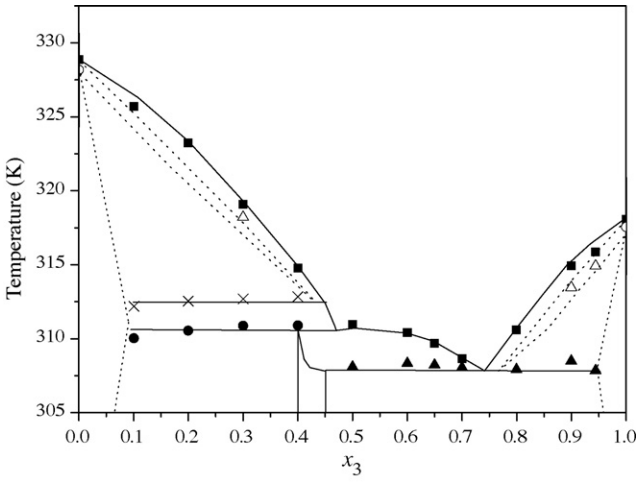

Fig. 12. Phase diagram of the system lauric acid (3) + myristic acid (4). (■) Fusion temperature; (●) peritectic temperature; (▲) eutectic temperature; (×) metatectic temperature; (△) transition temperature on the solid phase; (◯) transition on the solid phase of the pure component.

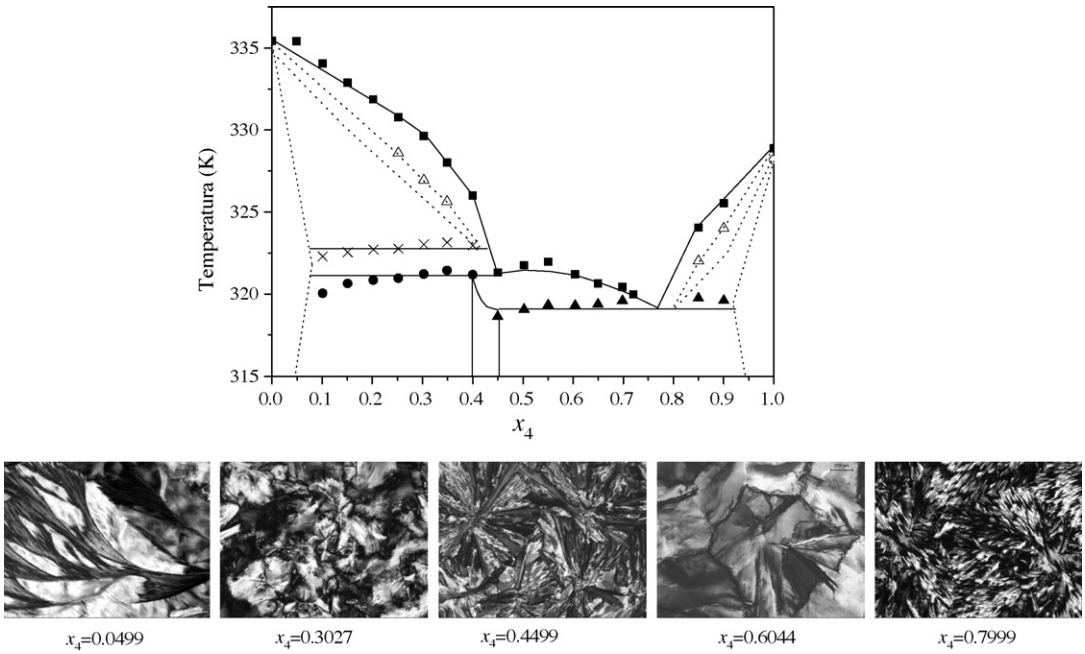

Fig. 13. Phase diagram of the system myristic acid (4) + palmitic acid (5) and light microscopy images of the same system at different compositions. (■) Fusion temperature; (●) peritectic temperature; (▲) eutectic temperature; (×) metatectic temperature; (△) transition temperature on the solid phase; (○) transition on the solid phase of the pure component.

The micrographs presented in Fig. 8 confirmed the existence of a biphasic region (C + l) between the peritectic temperature and the transition observed in the thermograms for 2–4 K above it. The inexistence of liquid in this region, as previously observed in the FT–Raman spectra, and now in the micrographs, showed that a metatectic reaction must be present in this system. The occurrence of a metatectic reaction explains the recrystallization observed in the micrographs and the absence of liquid at temperatures above the metatectic temperature, in a region where liquid should exist according to the conventional interpretation of the phase diagrams of these systems. A solid–liquid equilibrium region does exist, but only in a narrow temperature range close to the *liquidus* line.

The multiple phase regions at low temperatures identified by X-ray diffraction were also observed using polarized light microscopy, confirming the existence of five different domains at low temperatures.

With the combined results of the experimental techniques used in this work it was possible to show that the phase diagrams of these systems were not compatible with the type 2-Ib2 diagram previously proposed for these systems (Bailey, 1950; Small, 1986; Costa et al., 2007b). In accordance with previous results, eutectic and peritectic invariants were observed at concentrations of ≅0.7 and ≅0.5 molar fractions, respectively, for all the systems reported here. In addition to the peritectic and eutectic points, the following were also observed:

- Two metatectic invariants at concentrations not fully determined in this work but for which the temperatures were established for most of the systems studied. One of these was observed at a composition below the peritectic point and at a temperature ≅2–4 K above. The other metatectic point had a composition slightly superior to that of the eutectic and a temperature not much higher than that of the invariant point, which makes its detection quite difficult.
- There were five solid monophasic domains. Three of these were well established by the multiple techniques used, but the two domains associated with the metatectic point were very narrow and could not be individualized.
- Four solid–solid domains were observed along with five solid–liquid domains. The presence of all these two-phase domains was observed by the spectroscopic and microscopic techniques used here.

The phase diagrams of the systems studied in this work are reported in Figs. 10–14. They do indeed present a number of features similar to the phase diagrams of the binary system of dioic acids reported by Ventola et al. (2006), and are in good agreement with two recent works on the phase diagrams of binary mixtures of fatty acids that appeared during the revision process for this manuscript (Gbabode et al., 2008; Costa et al., 2009).

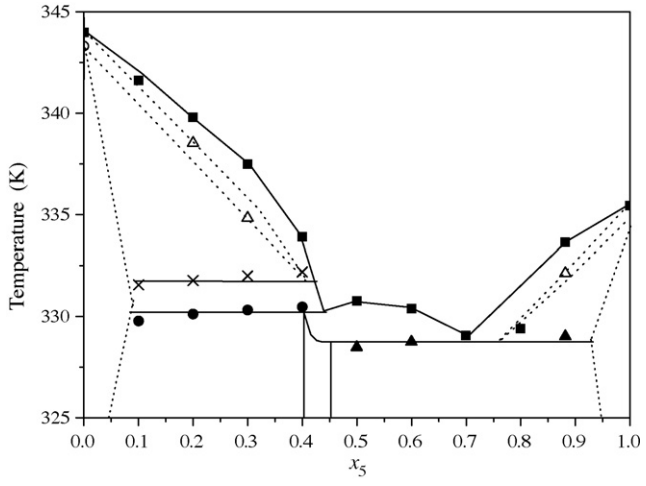

Fig. 14. Phase diagram of the system palmitic acid (5) + stearic acid (6). (■) Fusion temperature; (●) peritectic temperature; (▲) eutectic temperature; (×) metatectic temperature; (△) transition temperature on the solid phase; (○) transition on the solid phase of the pure component.

The metatectic reaction on the right hand side of the phase diagram was only observed for one of the systems studied, capric acid (2) + lauric acid (3), as shown in Fig. 11. Due to the proximity of the metatectic and eutectic temperatures, the peaks of these transitions overlapped, making it difficult to individualize the metatectic transition. It was also difficult to separate the transitions associated with the C_h monophasic regions. The presence of multiple regions in the phase diagrams at low temperatures was also observed, using polarized light microscopy, and the results were reported for the capric acid (2) + lauric acid (3) system in Fig. 11, and for the myristic acid (4) + palmitic acid (5) system in Fig. 13.

5. Conclusions

The solid–liquid phase diagrams for the binary mixtures of the saturated fatty acids formed by caprylic acid ($C_{8:0}$) + capric acid ($C_{10:0}$), capric acid ($C_{10:0}$) + lauric acid ($C_{12:0}$), lauric acid ($C_{12:0}$) + myristic acid ($C_{14:0}$), myristic acid ($C_{14:0}$) + palmitic acid ($C_{16:0}$) and palmitic acid ($C_{16:0}$) + stearic acid ($C_{18:0}$), were reported here for the first time.

Using differential scanning calorimetry complemented by X-ray diffraction, FT–Raman spectroscopy and polarized light microscopy measurements, it was possible to show that the conventional interpretation of these phase diagrams was not correct and to identify, in addition to peritectic and eutectic reactions, the occurrence of a metatectic reaction and regions of complete miscibility between the fatty acids at the extremes of the phase diagram and at intermediate concentrations. It was shown that, to the contrary of that previously admitted, the phase diagrams for these systems were quite complex, with important impacts on the design of separation and purification processes for fatty acids and also on the development of products based on these compounds.

Acknowledgments

The authors are grateful to CNPq (n° 141607/2004-1, 142823/2005-8 and 303649/2004-6), FAPESP (n° 2005/53095-2), CAPES-GRICES (0148/06-7), FAEPEX/UNICAMP, FEDER and the *Fundação para a Ciência e a Tecnologia* (project POCI/CTM/60288/2004) for their financial support.

References

Bailey, A.E., 1950. Melting and Solidification of Fats. Interscience Publishers, New York.
Becke, A.D., 1993. Density-functional thermochemistry. 3. The role of exact exchange. J. Chem. Phys. 98 (7), 5648–5652.
Brown, K.G., Bicknell-Brown, E., Ladjadj, M., 1987. Raman-active bands sensitive to motion and conformation at the chain termini and backbones of alkanes and lipids. J. Phys. Chem. 91, 3436–3442.
Carvalho, I.S., Miranda, I., Pereira, H., 2006. Evaluation of oil composition of some crops suitable for human nutrition. Ind. Crop Prod. 24 (1), 75–78.
Chapman, D., 1962. Polymorphism of glycerides. Chem. Rev. 62 (5), 433–456.
Costa, M.C., Krähenbühl, M.A., Meirelles, A.J.A., Daridon, J.L., Pauly, J., Coutinho, J.A.P., 2007a. High pressure solid–liquid equilibria of fatty acids. Fluid Phase Equilibr. 253 (2), 118–123.
Costa, M.C., Rolemberg, M.P., Boros, L.A.D., Krähenbühl, M.A., Oliveira, M.G., Meirelles, A.J.A., 2007b. Solid–liquid equilibrium of binary fatty acids mixtures. J. Chem. Eng. Data 52, 30–36.
Costa, M.C., Sardo, M., Rolemberg, M.P., Coutinho, J.A.P., Meirelles, A.J.A., Ribeiro-Claro, P., Krähenbühl, M.A., 2009. The solid–liquid phase diagrams of binary mixtures of consecutive, even saturated fatty acids: differing by four carbon atoms. Chem. Phys. Lipid 157, 40–50.
Chernik, G.G., 1995. Phase equilibria in phospholipid water-systems. Adv. Colloid Interfac. Sci. 61, 65–129.
Dorset, D.L., 2004. Crystallography of the Polymethylene Chain: An Inquiry into the Structure of Waxes. Oxford University Press, New York.
Falk, O., Meyer-Pittroff, R., 2004. The effect of fatty acid composition on biodiesel oxidative stability. Eur. J. Lipid Sci. Technol. 106 (12), 837–843.
Francis, F., Collins, F.J.E., Piper, S.H., 1937. The n-fatty acids and certain of their derivatives. Proc. R. Soc. A 158, 691–718.
Frisch, M.J., Trucks, G.W., Schlegel, H.B., Scuseria, G.E., Robb, M.A., Cheeseman, J.R., 2003. Gaussian 03, Revision B.04. Gaussian, Inc., Pittsburgh, PA.
Garti, N., Sato, K., 1989. Crystallization and Polymorphism of Fats and Fatty Acids. Marcel Dekker, New York.
Gbabode, G., Negrier, P., Mondieig, D., Moreno, E., Calvet, T., Cuevas-Diarte, M.A., 2008. Polymorphism and solid-state miscibility in the pentadecanoic acid-heptadecanoic acid binary system. Chem. Phys. Lipid 154 (1), 68–77.
Goto, M., Asada, E., 1978a. Crystal-structure of a-super form of lauric acid. Bull. Chem. Soc. Jpn. 51 (1), 70–74.
Goto, M., Asada, E., 1978b. Crystal-structure of b-form of stearic-acid. Bull. Chem. Soc. Jpn. 51 (9), 2456–2459.
Grondal, B.J., Rogers, D.A., 1944. Melting points of binary fatty acid mixtures C6 to C12 and their application in the determination of purity. Oil Soap. 21, 303–305.
Harihara, P., Pople, J.A., 1973. Influence of polarization functions on molecular-orbital hydrogenation energies. Theor. Chim. Acta 28 (3), 213–222.
Holland, R.F., Nielsen, J.R., 1963. A new crystal form of fatty acids. Acta Crystallogr. 16 (9), 902–906.
Inoue, T., Hisatsugu, Y., Ishikawa, R., Suzuki, M., 2004a. Solid–liquid phase behavior of binary fatty acid mixtures. 2. Mixtures of oleic acid with lauric acid, myristic acid, and palmitic acid. Chem. Phys. Lipid 127 (2), 161–173.
Inoue, T., Hisatsugu, Y., Suzuki, M., Wang, Z., Zheng, L., 2004b. Solid–liquid phase behavior of binary mixtures. 3. Mixtures of oleic acid with capric acid (decanoic acid) and caprylic acid (octanoic acid). Chem. Phys. Lipid 132, 225–234.
Inoue, T., Hisatsugu, Y., Yamamoto, R., Suzuki, M., 2004c. Solid–liquid phase behavior of binary fatty acid mixtures. 1. Oleic acid stearic acid and oleic acid behenic acid mixtures. Chem. Phys. Lipid 127 (2), 143–152.
Iwahashi, M., Takebayashi, S., Taguchi, M., Kasahara, Y., Minami, H., Matsuzawa, H., 2005. Dynamical dimer structure and liquid structure of fatty acids in their binary liquid mixture: decanoic/octadecanoic acid and decanoic/dodecanoic acid systems. Chem. Phys. Lipids. 133 (2), 113–124.
Johansson, J., Pettersson, S., Taylor, L.S., 2002. Infrared imaging of laser-induced heating during Raman spectroscopy of pharmaceutical solids. J. Pharmaceut. Biomed. 30 (4), 1223–1231.
Johnson, R.W., Fritz, E., 1989. Fatty Acids in Industry: Processes, Properties, Derivatives, Applications. Marcel Dekker, Nova York.
Kaneko, F., Kobayashi, M., Kitagawa, Y., Matsuura, Y., 1990. Structure of stearic-acid e-form. Acta Crystallogr. C 46, 1490–1492.
Karleskind, A., 1996. Oils & Fats Manual: A Comprehensive Treatise, Properties, Production, Applications. Lavoisier Publishing, Paris.
Kogan, A., Garti, N., 2006. Microemulsions as transdermal drug delivery vehicles. Adv. Colloid Int. Sci. 123, 369–385.
Lee, C.T., Yang, W.T., Parr, R.G., 1988. Development of the Colle-Salvetti correlation-energy formula into a functional of the electron-density. Phys. Rev. B 37 (2), 785–789.
Lewis, R.N.A.H., McElhaney, R.N., 2000. Vibrational spectroscopy of lipids. In: Chalmers, J.M., Griffiths, P.R. (Eds.), Handbook of Vibrational Spectrsocopy, vol. 5. John Wiley & Sons, New York, pp. 3447–3464.
Lomer, T.R., 1963. Crystal and molecular structure of lauric acid (form a1). Acta Crystallogr. 16 (10), 984–988.
Marigheto, N.A., Kemsley, E.K., Potter, J., Belton, P.S., Wilson, R.H., 1996. Effects of sample heating in FT–Raman spectra of biological materials. Spectrochim. Acta A 52 (12), 1571–1579.
Meher, L.C., Sagar, D.V., Naik, S.N., 2006. Technical aspects of biodiesel production by transesterification—a review. Renew. Sust. Energ. Rev. 10 (3), 248–268.
Moreno, E., Cordobilla, R., Calvet, T., Cuevas-Diarte, M.A., Gbabode, G., Negrier, P., Mondieig, D., Oonk, H.A.J., 2007. Polymorphism of even saturated carboxylic acids from n-decanoic to n-eicosanoic acid. New J. Chem. 31, 947–957.
Müller, E., Stage, H., 1961. Experimentelle vermessung von dampf-flüssigkeits-phasengleichgewichten. Springer, Berlin.
Nolasco, M.M., Amado, A.M., Ribeiro-Claro, P.J.A., 2006. Computationally-assisted approach to the vibrational spectra of molecular crystals: study of hydrogen-bonding and pseudo-polymorphism. Chemphyschem 7 (10), 2150–2161.
Nývlt, J., 1977. Solid–Liquid Phase Equilibria. Elsevier, Amsterdam.
Sato, K., 2001. Crystallization behaviour of fats and lipids—a review. Chem. Eng. Sci. 56, 2255–2265.
Sato, K., Ueno, S., Yano, J., 1999. Molecular interactions and kinetic properties of fats. Prog. Lipid Res. 38 (1), 91–116.
Scott, A.P., Radom, L., 1996. Harmonic vibrational frequencies: an evaluation of Hartree–Fock, Moller–Plesset, quadratic configuration interaction, density functional theory, and semiempirical scale factors. J. Phys. Chem. 100 (41), 16502–16513.
Shilei, L., Neng, Z., Guohui, F., 2006. Eutectic mixtures of capric acid and lauric acid applied in building wallboards for heat energy storage. Energy Buildings 38, 708–711.
Small, D.M., 1986. Physical Chemistry of Lipids: From Alkanes to Phospholipids. Plenum Press, New York/London.
Tandon, P., Forster, G., Neubert, R., Wartewig, S., 2000. Phase transitions in oleic acid as studied by X-ray diffraction and FT–Raman spectroscopy. J. Mol. Struct. 524, 201–215.
Timms, R.E., 1984. Phase behaviour of fats and their mixtures. Prog. Lipid Res. 23, 1–38.
Vand, V., Morley, W.M., Lomer, T.R., 1951. The crystal structure of lauric acid. Acta Crystallogr. 4 (4), 324–329.
Vaz, P.D., Ribeiro-Claro, P.J.A., 2005a. C—(HO)—O—. . . hydrogen bonds in small ring carbonyl compounds: vibrational spectroscopy and ab initio calculations. Struct. Chem. 16 (3), 287–293.

Vaz, P.D., Ribeiro-Claro, P.J.A., 2005b. The role of C–H center dot center dot center dot O interactions in the solid and liquid-phase structures of methyltrioxo rhenium. Eur. J. Inorg. Chem. (10), 1836–1840.

Ventola, L., Bayes, L., Benages, R., Novegil-Anleo, F.J., Cuevas-Diarte, M.A., Calvet, T., Mondieig, D., 2008. Decanedioic acid (C10H18O4)/dodecanedioic acid (C12H22O4) system: polymorphism of the components and experimental phase diagram. Helv. Chim. Acta 91, 1286–1298.

Ventola, L., Metivaud, V., Bayes, L., Benages, R., Cuevas-Diarte, M.A., Calvet, T., Mondieig, D., 2006. The binary system tetradecanedioic acid-hexadecanedioic acid: polymorphism of the components and experimental phase diagram. Helv. Chim. Acta 89 (9), 2027–2039.

Zhang, J.J., Zhang, J.L., He, S.M., Wu, K.Z., Liu, X.D., 2001. Thermal studies on the solid–liquid phase transition in binary systems of fatty acids. Thermochim. Acta 369 (1–2), 157–160.